1

Introduction to Heat Transfer During the Forming of Organic Matrix Composites

In this chapter, we present some very illustrative examples of advances obtained in the analysis of the heat transfer in the forming processes of composites. These examples highlight at the same time the difficulties and scientific issues, as well as some simplified approaches to obtain, in an accessible way, a rapid estimation of the times of cooling or heating of a composite part. We also point out some preconceived ideas, in particular on the nature of transfers during the filling of molds in injection process, and for this we propose a new criterion to determine the transition between the thermal shock regime and the one of established convection, which is validated by experimental results. The selected processes are the injection of composites with short fibers (thermoplastic and thermosets), and the injection on a fabric. The examples are illustrated by results issued of more than 25 years of analysis of heat transfer in the processes, during thesis led within the framework of partnership programs with companies of the plastics processing industry. Finally, some directions for new developments are proposed.

1.1. Introduction

The mastery of composite forming processes raises a number of challenges on heat transfer and how to take them into account adequately. Indeed, the nature of these materials itself induces peculiarities. First, they have at least two components, which poses the problem of determining their effective properties according to those constituents. Composites are also multi-scale materials: the fibers are gathered into tows, which are woven to make a fabric. Reinforcements, but sometimes also the matrices, are anisotropic. The coupled phenomena introduce complex physics difficult to interpret without thorough knowledge of them and their interactions. Furthermore, the operating conditions in the process can be often considered as extreme. High cooling rates are frequently encountered, such as for the contact

Chapter written by Didier DELAUNAY.

between a cold mold and a hot composite. Shear rates can be very large at the wall of an injection mold, or in the micro channels between fibers (even if the flow rates are low). To compensate the shrinkages due to the cooling or the transformations, pressures are sometimes very high in the molding cavity (up to 200 MPa for injection). Low-conductive polymers and composites are in some cases subjected to overheating as a result of heat source release induced by transformation. An additional issue is the fact that the temperature measurement is very difficult because it is intrusive. It is not yet well known how to experimentally determine the temperature fields within a molded part or inside of the plies in a reinforcement stack. The size of thermocouples, which should be at least as small as the fibers, makes them very fragile, especially in a viscous fluid flow. To date, the precise determination of the inlet temperature in the injection channel of a mold is an open problem. Another particularly characteristic example is the location of the filling fronts and the saturation distribution in a composite made by liquid composite molding (LCM) since it is coupled to heat transfer. In addition, solving a heat transfer problem requires the accurate knowledge of the boundary conditions, which may be difficult. We can also give the example of the determination of the thermal contact resistance (TCR) to the wall of a molding cavity or between plies during the consolidation of a composite.

Temperatures are important to know, but the dynamics of a thermal system may be assessed only by measuring the heat flux. How to make a heat flux sensor non-intrusive and accurate in the environment of forming processes? The main question is ultimately whether a fine thermal knowledge is essential to achieve quality parts.

In this chapter, we will show, from a few illustrative examples, that the couplings involved at all levels must be adequately taken into account from the point of view of heat transfer, since they induce consequences on the quality of the final product appearance, size, shape and properties. The thermal scientific problem appears as inevitable, especially since productivity requires short cycles in mass production: there is indeed cycles of about 1 min for automotive parts. Everyone can easily understand that the heating and cooling of a part by varying its temperature sometimes several hundred degrees in very short times, with the objective to control the temperature fields and to obtain uniform final properties for complex shapes, requires a non-trivial strategy.

1.2. Examples of injection of short fiber reinforced composites

1.2.1. *Heat transfer during the filling phase*

1.2.1.1. *Case of semi-crystalline polymer matrices*

We will first discuss the injection of a polymer reinforced with glass fibers, taking the example of a widely distributed poly-aramid, whose trade name is IXEF

[PIN 09]. The scope of this study is a collaborative program ("FISH" program) involving LTN, IMP (Lyon), PIMM (ENSAM Paris) laboratories and Moldflow, Legrand, and Solvay companies.

An injection cycle is typically divided into four phases: the filling step (few seconds) is short compared to the total cycle time, during which high shear rates may occur. The packing phase consists of applying a pressure on the polymer/composite to compensate the thermal and crystallization shrinkages. The third step is the isochoric cooling under pressure after the gel of the injection gate, preventing the entry or exit of polymer from the molding cavity and finally the cooling at atmospheric pressure after the possible unsticking of the part. At the end of the cooling, the solid polymer part is ejected and the new cycle can begin.

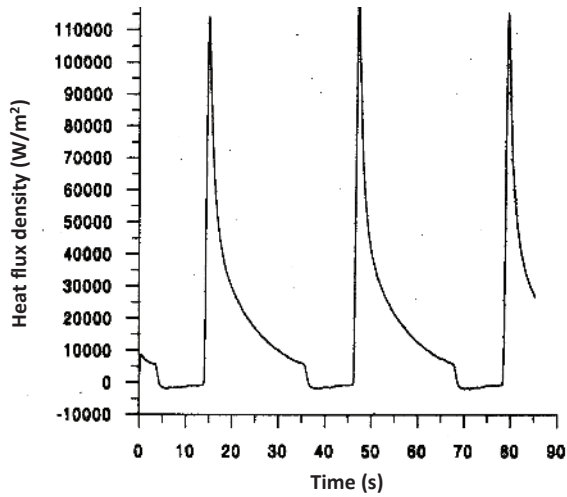

Figure 1.1. *Heat flux to the wall of a molding cavity in injection process*

The thermal behavior of the mold is periodic: the heat flux exchanged between the part and the mold is very large at the beginning of the cycle, decreases and finally is negative at the ejection, as shown in Figure 1.1. This particularity has to be taken into account since an established periodic state is required for constant quality parts. The typical example of heat flux at the wall of a molding cavity displayed in Figure 1.1 highlights a dramatic and very quick decrease. How can we interpret this behavior? Let us consider the flow in the channel formed by the molding cavity. If we assume legitimately that the forced convection is in the steady

state, it is possible under these conditions to evaluate a local Nusselt number at the distance x from the entry of the molding cavity using a conventional correlation for a prescribed wall temperature [PIN 09], for a shear thinning fluid with a rheological power law type:

$$Nu(x) = 1.16((3n + 1)/4n)^{1/3} (PeD_h/x)^{1/3} \quad [1.1]$$

The Peclet number is defined as $Pe = VD_h/a$; D_h is the hydraulic diameter of the channel, here twice its thickness, a is the diffusivity of melt, n is the index of the power law viscosity. For the considered instrumented molding cavity [LEG 06] (incomplete part is shown in Figure 1.2 and instrumented cavity in Figure 1.10), we obtain the position of the sensor near the gate a value of 20 for the Nusselt number, which corresponds to a constant heat flux during the filling phase close to 1.10^5 W/m^2. The heat flux obtained as such (see detailed calculations in section 1.2.1.2 applied for bulk molding compound (BMC) processing) is the good order of magnitude (see Figure 1.1) but the experimental one decreases very quickly and we do not observe a constant value even during a short time. The analysis is thus invalidated: the evolution of the heat flux does not correspond to a regime of established convective exchange between the polymer and the wall of the molding cavity. Here is a preconceived idea, which constitutes an approach nevertheless classic but erroneous.

Let us test then the hypothesis that the heat flux decrease is due to the coupling with the conduction in the mold. There is an analytical solution [CAR 59] to the problem of a flowing fluid, which is suddenly put into contact with a wall. In this solution, exchanges by convection are based on a constant convective heat transfer coefficient h. This latter, calculated from the equations [1.1] and [1.11], is in this case approximately equal to 660 W/m^2/K (we take the value n = 0.308). The heat flux density is given by $\Phi(t) = h\, F(t/\tau)\, (T_m - T_i)$. T_m is the average temperature of the melt, and T_i is the initial temperature of the mold. F is a decreasing function of time [CAR 59]. τ is given by $\tau = \lambda^2/h^2 a$, where λ is the mold thermal conductivity and a is the melt diffusivity. For the molding cavity studied, we find $\tau = 35586$ s, which corresponds to about 10 h. The rapid decrease in the observed heat flux is completely incompatible with this law since for $t = \tau$ the value of the function F is approximately 0.4. The result of this analysis using *a reductio ad absurdum* that convective heat transfer during the filling phase is not the key to analyze the heat transfer with the mold.

Let us consider the incomplete part shown in Figure 1.2. The energy equation for the filling of the molding cavity may under certain simplifying assumptions (constant thermophysical properties in particular) be written as:

$$\rho C_p DT/Dt = \beta TDP/Dt + \eta\dot{\gamma}^2 + \lambda\, \Delta T + Q \quad [1.2]$$

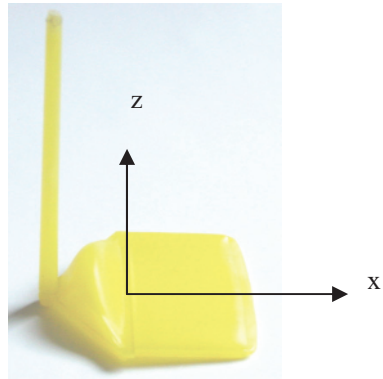

Figure 1.2. *Incomplete part obtained with the SWIM mold [LEG 06]*

In this equation, D/Dt is the operator ($\partial/\partial t$ + V.grad). The left term represents the thermal inertia. The first term on the right is due to the compressibility. The analysis of its order of magnitude shows that in first approach, it can be neglected. The second term is due to the viscous dissipation. Although it is not always negligible, it is also an order of magnitude lower than the other terms, especially early in the filling phase. The third term is the thermal diffusion, which occurs mainly in the z direction. Q is the possible source due to the phase change of the polymer (in the case of semi-crystalline thermoplastics, for example). A commonly accepted hypothesis is that transfers are one-dimensional (1D) along z, so that we can neglect viscous dissipation and the effect of the compressibility. Equation [1.2] can be thus simplified:

$$\rho C_p(\partial T/\partial t + v_x\, \partial T/\partial x) = \lambda\, \partial^2 T/\partial z^2 \qquad [1.3]$$

The second term of the left side equation [1.3] is, at the beginning of the filling phase, of several orders of magnitude, lower than the first one. Indeed, the term $\partial T/\partial t$ is very large and takes precedence over the other. We can then neglect this one and the equation is reduced to the classical 1D Fourier equation:

$$\rho C_p \partial T/\partial t = \lambda\, \partial^2 T/\partial z^2 \qquad [1.4]$$

The part is then subjected to a heat shock: for a short time (fast filling), it can be assumed that during this stage only the surface layers of the part and the mold in the vicinity of the wall of the molding cavity are involved in heat exchanges. The temperature field is thus the one observed in two semi-infinite media suddenly put

into contact. At this time, the temperature in the polymer can be assumed to be uniform and equal to the injection temperature T_{inj}. The temperature in the vicinity of the molding cavity wall is quasi-uniform and equal to the temperature of the mold surface at the time of the beginning of the filling phase. We denote it by T_{mi}. The solution of the contact problem is well known. In the case of an amorphous polymer, if we neglect the contact resistance between the mold and the polymer, the mold surface temperature T_c at the contact time is given by equation [1.5]

$$T_c = (T_{inj}b_p + T_{mi}b_m)/b_p + b_m) \quad [1.5]$$

In this equation, b_p and b_m denote, respectively, the effusivity of the polymer and the mold, given by the square root of the product thermal conductivity λ, volumic mass ρ and specific heat C_p: $b = (\lambda\rho C_p)^{0.5}$. Let us apply this result on the example presented in Figure 1.3, where the time evolution of the mold surface temperature is plotted for the injection of an ABS in a steel mold. The thermal properties of this steel are $\lambda = 36$ W.m^{-1}.K^{-1}, $\rho = 7850$ kg.m^{-3}, $C_p = 460$ J.kg^{-1}.K^{-1}.

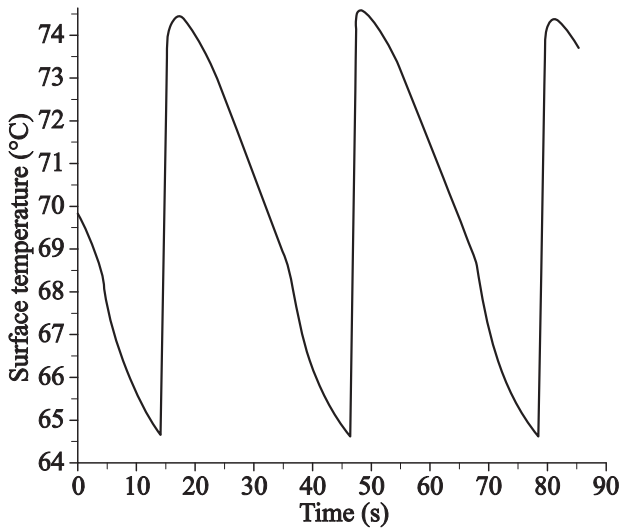

Figure 1.3. *Surface temperature of a mold during injection of an amorphous polymer (ABS)*

The injection temperature of the molten polymer is 240°C. In a periodic regime, we can see that the experimental temperature of the injection mold, which is the

minimum value of the curve, is about 64.7°C. The effusivity of the mold steel is 11,474 $J.K^{-1}.m^{-2}.s^{-1/2}$. The ABS used for this test had the following properties: thermal conductivity $\lambda = 0.2$ $W.m^{-1}.K^{-1}$, density $\rho = 961$ $kg.m^{-3}$, specific heat $C_p = 2{,}300$ $J.kg^{-1}.K^{-1}$. Its effusivity is, therefore, 665 $J.K^{-1}.m^{-2}.s^{-1/2}$. From equation [1.5], the contact temperature is equal to $T_c = 74.3$°C. This value is obviously very close to the recorded maximum temperature reached by the molding cavity surface, which corresponds to the time of contact of the mold with the hot polymer. This first result is in line with the validation of the heat shock phenomenon governed by the conduction in the part thickness. We note a temperature range of 10 K for the increase in the wall temperature. This result is classic. Soon after, the temperature decreases, because the condition of semi-infinite medium is only valid in the first times of the cycle for a dimensionless characteristic time $\tau = at/e^2 <$ 0.05 (empirical result). In the expression of τ, a is the thermal diffusivity of the polymer and e is the half-thickness of the part. In our case, $e = 1.5.10^{-3}$ m and the diffusivity of the ABS is $9.10^{-8} m^2.s^{-1}$. The corresponding time below which the assumption of infinite medium is valid is 1.25 s. From the end of the filling that lasts 1 s, the core temperature of the part decreases and, as a result, the surface temperature.

The heat flux exchanged between the part and the mold associated with equation [1.5] is decreasing and is given by:

$$\Phi(t) = \lambda (T_{inj} - T_c)/\sqrt{\pi a t} \qquad [1.6]$$

This expression of the heat flux, inversely proportional to the square root of the time, is consistent with the experimental observation. It was compared with the experimental data recorded during the injection of an isotactic polypropylene [LEB 98]. Figure 1.4 illustrates the good description of the experimental heat flux by this law during the filling phase, within the first second after contact, when the polypropylene is in the molten (and thus amorphous) state. Then, the beginning of the crystallization is observed, since it induces an increase in the heat flux. At this time, the model deviates from the experiment since it cannot take into account the effect of the phase change. This result completes the demonstration that in the early time of the injection cycle, conductive thermal shock allows us to interpret perfectly the heat exchanges between the part and the mold. Is it possible to transpose this result to a charged polymer, additionally for a semi-crystalline one?

The first approach is to consider the neat matrix. Figure 1.5 displays a typical example of the wall temperature of the molding cavity for the injection of a semi-crystalline polymer [SOB 13].

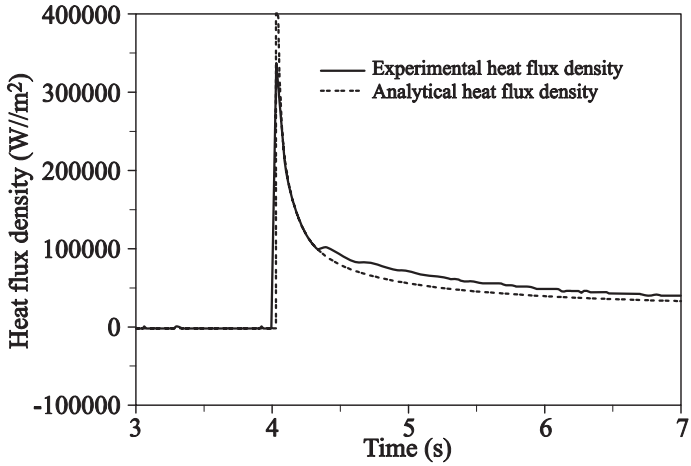

Figure 1.4. *Comparison between the heat flux given by equation [1.6] (dotted line) and the measurement (solid line) in thermal shock regime during the injection of an isotactic polypropylene [LEB 98]*

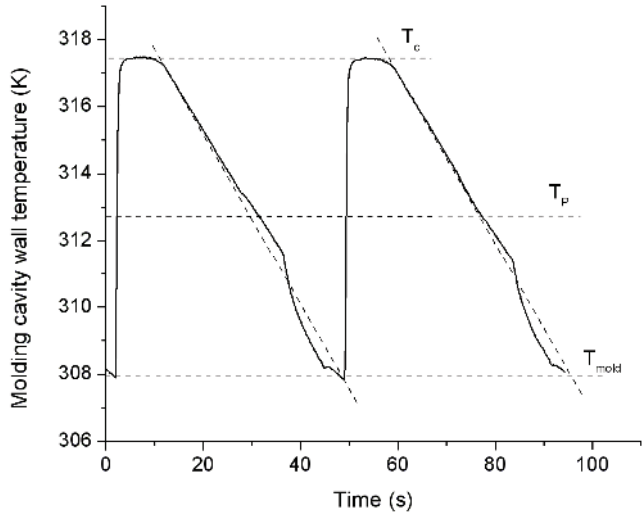

Figure 1.5. *Wall temperature in the molding cavity during the injection of isotactic polypropylene [SOB 13]*

Unlike amorphous polymers, we observe that the temperature curve shows a net plateau during the first seconds before the decreasing due to cooling. This is due to

the latent heat of crystallization. The solution of a thermal shock problem with phase change (Stefan problem [SOB 13]) induces a change (in comparison with the classical case) of the contact temperature equation [LOU 97]:

$$T_c = \frac{b_s T_F + b_m erf(\xi/\nu) T_{mi}}{b_s + b_m erf(\xi/\nu)} \qquad [1.7]$$

In this relation, $\nu = \sqrt{a_s/a_l}$ where a_s and a_l are the solid and liquid (i.e. molten) phases diffusivity, respectively. ξ is the solution of the transcendental equation

$$Ste_s \nu \frac{e^{-\xi^2/\nu^2}}{erf(\xi/\nu)} - \frac{Ste_l e^{-\xi^2}}{erfc(\xi)} = \sqrt{\pi}\xi \quad ; \quad t > 0 \qquad [1.8]$$

where $Ste_l = Cp_l(T_{inj} - T_F)/L$, $Ste_s = Cp_s(T_F - T_c)/L$ are, respectively, the liquid and solid Stefan numbers. T_F is defined as the temperature of the crystallization quasi-plateau that appears in the core of the polymer upon cooling [SOB 13]. This is a new thermophysical characteristic, which depends on the pressure conditions. It can be determined experimentally or by simulation taking into account the kinetics of crystallization and its changes under pressure. The iterative solution of equations [1.7] and [1.8] allows calculating ξ and T_c. The quasi-plateau observed in the core of the part is related to the heat released during the crystallization, maintaining T_F until the complete solidification. Therefore, the constant half-thickness temperature is imposed, which has the effect to extend the semi-infinite character of the phenomenon, hiding what happens "behind" the isotherm T_F. This plateau, therefore, lasts until complete solidification of the part. What happens if we add short fibers to the semi-crystalline polymer?

Figure 1.6 shows a typical example of the evolution of the mold surface temperature during the injection of a poly-aramide reinforced with short glass fibers. A temperature plateau is clearly observed and its time is even longer than the reinforcement ratio is low. This is related to the solidification time since the latent heat decreases when the reinforcing ratio increases. The plateau temperature is also even higher than the reinforcing ratio increases. It can be explained by the increase in the contact temperature induced by both the increase in ξ, when latent heat decreases (the solidification is faster) and the increase in the effusivity of the composite when the glass fiber weight ratio is higher. The accurate calculation of T_c confirms these effects and the experimental results. 1D heat transfer in the composite through the thickness of the part has been demonstrated in several studies

[DEL 11, LEG 10, LEG 11], the fibers being oriented in the part in a core-skin structure.

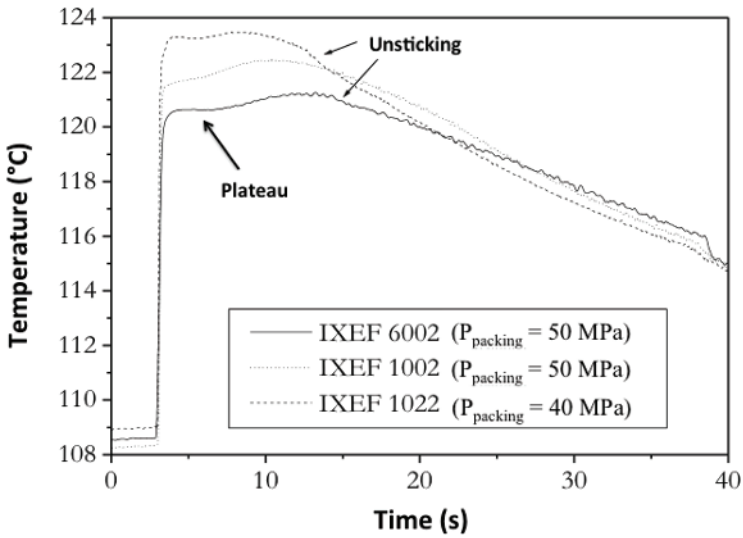

Figure 1.6. *Molding cavity wall temperature during the injection of poly-aramide composites [LEG 06]: no fiber (IXEF 6002), 30 wt% fiber (IXEF 1002), 50 wt% (IXEF 1022)*

This characteristic behavior has the advantage of applying the method described in [SOB 13] to easily estimate the cooling time of the composite part and thus to choose the optimum molding parameters. Indeed, observing Figure 1.6, we note that the molding cavity surface temperature may be less than 1 K with accuracy schematically described by successively a plateau (ordinate T_c) and the negative slope line connecting the point corresponding to the solidification time with ordinate T_c (120.5°C for IXEF 6002) to the point corresponding to the part ejection (39 s, 116.5°C for IXEF 6002). The solidification time may be calculated analytically [SOB 13]. It is then possible to analytically calculate the temperature changes in the part and therefore the time for which an ejection criterion is reached. Needless to say that such a simplified approach is not a substitute for professional software that continuously become more accurate, as Moldflow© for example, but it provides the expert with a relatively precise and very quick estimate. This reduced model is also an advantage for optimization software that uses intensively direct problems for solving.

1.2.1.2. *Bulk molding compound injection molding*

This section is dedicated to research work done as part of a program with the ultimate goal of controlling surface aspect of parts made of BMC, involving several laboratories: CRMD of Orleans, the Department of Polymers and Composites Technology of the School of Mines of Douai, LTN laboratory and Menzolit company (now known as IDI Composites), material supplier. Our specific goal in this study that covered several cooperative programs between 1997 and 2003 was to better control heat transfer in the injection of these composites constituted of unsaturated polyester resin, thermoplastic additive (to compensate the shrinkage induced by the crosslinking), mineral fillers and short glass fibers. The results are detailed in [MIL 01]. An experimental mold equipped with pressure and heat flux sensors was designed, as shown in Figure 1.7.

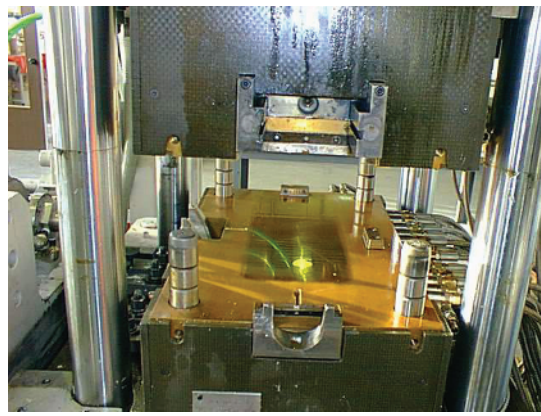

Figure 1.7. *Picture of the instrumented mold for the heat transfer study of the injection of a BMC plate*

This mold was mounted onto a vertical press (200 tons clamping force). The injection unit is horizontal. It is equipped with heating elements to heat the material up to 40°C in order to reduce its viscosity, which facilitates its injection. A water-cooled nozzle avoids the warming induced by the hot mold. Material gelation in the nozzle is then avoided. The injected part had a size enough large to be representative of the process: 0.4 m × 0.15 m × 3 mm. The heating channels of the mold are such that the thermal gradient along the walls of the molding cavity is as small as possible. An oil regulator unit is used to heat the mold up to 180°C. Two pressure sensors and four thermal ones (heat flux and temperatures) have been placed into the mold according to the positions indicated in Figure 1.8. The pressure sensors are Kistler type. Data acquisition is done by a Tektronix recorder (200 measures/s). The heat flux sensors conception and their manufacturing have been done in our

laboratory [QUI 98] and are composed of three small thermocouples (25 µm diameter). Each sensor is made with the same steel (Z40CDV3) as the mold so that it is fully non-intrusive from a thermal point of view. A numerical treatment of the data (using the 1D sequential inverse method of Beck [SOM 12]) gives the temperature and the flux density at the sensor surface. Practically speaking, the thermocouple placed far (4.9 mm in our case) from the surface defines the boundary condition; the two others are used for the criterion calculation. This criterion is defined as the quadratic difference between the calculated temperatures (for the position of each thermocouple) and the measured ones. The minimization of the criterion gives the surface heat flux density and the temperature evolution with time. Theoretically, two thermocouples are sufficient for calculation. However, the analysis with three thermocouples gives a better confidence in the results. The thermophysical properties of the steel have been carefully measured due to classical methodologies. Note that short fibers are all oriented in the plane of the part, so that heat transfer arises mainly in the direction of the thickness of the sample. The heat flux sensors have a time constant lower than 5 ms. Indeed, the thermocouples are semi-intrinsic with separated junctions. The metal of the sensor itself ensures the electric continuity. The sensor thermocouples are K type (the thermoelectric power of about 40 µV/°C). This low voltage generates acquisition difficulties and amplification of the signal is necessary.

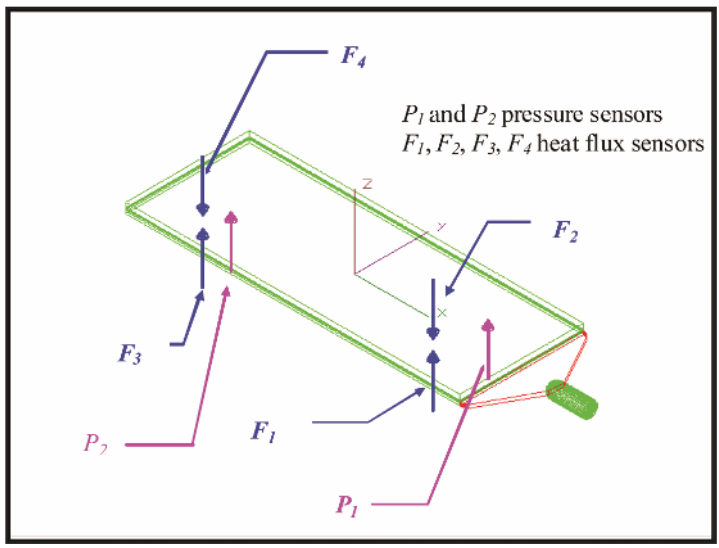

Figure 1.8. *View of the BMC part indicating the locations of the sensors*

A characteristic result of heat flux and pressures during the filling phase is shown in Figure 1.9 and we intend to use it to illustrate the power of relevant thermal analysis. The mold temperature before the injection is set to 140°C, whereas the BMC is maintained at 40°C in the injection unit. During the injection, when the material arrives in front of the heat flux sensors F1 and F2, the heat flux decreases sharply, nevertheless increasing in absolute value. We note that between 0.40 and 0.45 s, the sensors facing each other (one on top of the mold and the other on the lower part) have different responses. This is due to a particularity of the BMC injection, which is also observed in some cases of fiber-reinforced thermoplastics: the existence of a "non-sticking front" ahead of the front. BMC is a yield stress fluid, implying that it has a "piston-type" flow until the velocity and duration of shear is not high enough (with respect to the yield stress). It does not adhere to the wall of the molding cavity. Therefore, there is no contact on the sensor F2 that does not see the front, while there is a poor contact on the sensor of the lower mold part (i.e. F1). Both curves of heat flux F1 and F2 converge after 0.05 s to a maximum absolute value before rising up to an injection time equal to 0.6 s. This initial change is characteristic of a heat shock regime with imperfect contact between the "cold" BMC and the hot mold. From t = 0.6 s, the heat flux given by the sensors F1 and F2 stabilizes at almost the same value. The mold is relatively long and, unlike the case of thermoplastics, there is time to reach an established convective regime.

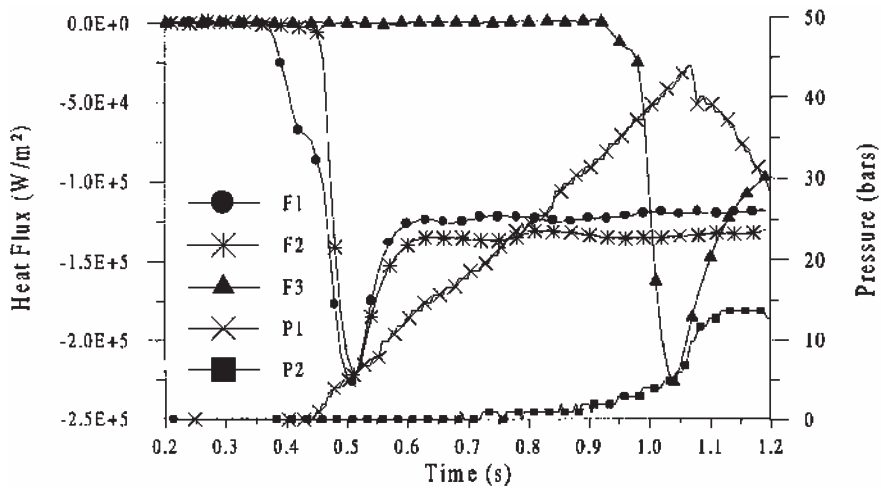

Figure 1.9. *Characteristic record of the heat flux and pressure during the filling of the mold*

The same behavior is observed on the F3 sensor at the bottom of the molding cavity, the maximum magnitude of the heat flux being the same as on the sensors

near the injection gate. The composite was not heated significantly during its flow in the mold. This hypothesis is confirmed by the observation of the given pressure P1 by the sensor: the linear evolution during the filling is correlated to the increase in the pressure drop between the sensor position and the BMC front, the filling taking place with a constant flow rate. The fact that the slope is constant reflects that the variation of the viscosity, and therefore the composite average temperature, are almost negligible.

Therefore, heat flux sensors are excellent detectors of events and these data may be used to initially test the rheology of the composite. Indeed, while with the pressure sensors it is difficult to detect the passage front of the material (particularly with P2 sensor), we can estimate the filling velocity by identifying, for example, the minimum flux on the sensors F2 and F3. The distance between these sensors is 0.273 m, and the peaks are separated by 0.55 s. The result is an average velocity $\overline{V}$ = 0.496 m.s^{-1}.

Rheological measurements [MIL 01] demonstrate that the rheological behavior can be modeled with an Oswald–de Waelde-type shear thinning model $\eta = K(T)\ \dot{\gamma}^{m-1}$ with m = 0.43 and K(T) = 7600.4 exp(–0.025T). This is consistent with what is proposed in [LE 07]. Let us consider the filling of the molding cavity between the sensor locations, defining a channel of width W considered as infinite, with a length L = 0.273 m, and a height h = 3.10^{-3} m. The flow is therefore in this two-dimensional (2D) channel. The volume flow rate is expressed by:

$$Q = \overline{V}hW \qquad [1.9]$$

Given the rheological law of the BMC, the volumetric flow rate is classically given by:

$$\frac{m}{2(2m+1)}\left(\frac{1}{2K}\frac{\Delta P}{L}\right)^{1/m} h^{\frac{1+2m}{m}} W = Q \qquad [1.10]$$

From equations [1.9]–[1.10], taking into account values of m and h, $\overline{V}$ can be inferred from the value of ΔP and the apparent value of the consistency index K(T): the mold can be viewed as a sort of rheometer. As shown in Figure 1.9, the pressure increases from 5 to 40 bars between 0.5 and 1.05 s, i.e. a pressure variation equal to 3.5 10^6 Pa. We thus determine at the average temperature the fluid composite consistency index: $K(T_{inj})$ = 8.54 10^2 Pa.s. Using the classical expression of the apparent shear rate $\dot{\gamma}_a = 6Q/Wh^2$, we obtain a value $\dot{\gamma}_a$= 1,000 s^{-1}. Using the expression of the viscosity given above, the apparent viscosity of the uncured composite would be η_a = 16.65 Pa.s. The laminar 2D flow in the mold is an advantage to characterize *in situ* the composite and to compare the results with

laboratory techniques, which are unfortunately not always appropriate. The aging of the polymer can thus be identified by changes in viscosity.

Let us go further into the analysis and try to quantify the heat flux at the molding cavity wall, in the steady convective regime (in the plateau between 0.6 and 1.2 s). For this purpose, we use the classical correlation given in equation [1.1]. The Peclet number value is $Pe = \overline{V}D_h/a$ where a is the thermal diffusivity. We noted the fiber orientation is in the flow plane (in this plane, they exhibit an orientation distribution in x and y directions indicated in Figure 1.8). The transverse thermal conductivity, measured in guarded hot plate, was found independent of temperature and equal to $\lambda = 0.6$ W.m^{-1}.K^{-1} whereas the density is 2,000 kg.m^{-3} and the specific heat is 1,200 J.Kg^{-1}.K^{-1}. BMC diffusivity is then $2.5.10^{-7}$ m^{2}s^{-1}. The hydraulic diameter D_h being equal to 2 h, so we deduce $Pe = 1.2.\ 10^4$. The F1 and F2 sensors are located 67 mm from the injection gate. This singularity is thus the origin of the thermal boundary layer. We obtain by applying the formula given in equation [1.1], taking the origin of x at the injection gate, the value of the Nusselt number to the position of the sensor $Nu(x = 67.10^{-3}m) = 12.77$. Then, we can deduce the heat transfer coefficient by equation [1.11]:

$$h\ (x = 67.10^{-3}m) = Nu\ \lambda\ /D_h \qquad [1.11]$$

We obtain the value $h = 1277$ W.m^{-2}.K^{-1}. The heat flux density is then given by:

$$\Phi = h\ (\ T_p - T_{inj}\ ) \qquad [1.12]$$

where T_p represents the average temperature of the molding cavity wall during the filling step; $T_p = 132$°C between 0.5 and 1.2 s at 132°C for the sensor F2 and $T_p = 130$°C for the sensor F1. The corresponding heat flux is in absolute value $1.18.10^5$ W.m^2.K^{-1} for sensor F2 and 1.15 W.m^2.K^{-1} for sensor F1. Experimentally, the sensors record the entering heat flux in the mold as negative because the hot mold transfers the heat to the cold composite ($T_{inj} = 40$°C). Experimental absolute values given in Figure 1.9 are very close to the values estimated by equations [1.1], [1.11]–[1.12] (better than 10% accuracy for the predicted heating). Calculations also indicate that the heat flux given by F2 is greater than F1 in absolute value. The heat flux estimation is of great interest because conversely, it allows calculating the average temperature in the part thickness from a heat balance during the residence time in the mold. As such, we can build simplified models for heat transfer.

Nevertheless, a question arises on the transition into the mold between the heat shock regime and the convective flow regime. An attempt to estimate this time can be to find the time for which the conductive heat flux due to thermal shock decreasing in $1/\sqrt{t}$ (equation [1.6]) becomes equal to the steady regime of convective heat flux given by equations [1.1], [1.11–1.12].

Conductive heat flux during a thermal shock is given by equation [1.6]. Equations [1.11]–[1.12] combined with the expression of the Nusselt number in a plane channel (equation [1.1]) are used to calculate the convective flux. By identifying these two expressions, and by dividing both sides of the equality by λ ($T_{inj} - T_c$), we obtain equation [1.13] where x is the distance between the gate and the position of the sensor:

$$\frac{1}{\sqrt{\pi at}} = \frac{1.276}{D_h}\left(\frac{3m+1}{4m}\right)^{\frac{1}{3}}\left(\frac{PeD_h}{x}\right)^{\frac{1}{3}} \quad [1.13]$$

For the BMC, the index of the power law being m = 0.43, this previous expression becomes:

$$\frac{at}{D_h^2} = 0.1955\left(\frac{x}{Pe.D_h}\right)^{\frac{2}{3}} \quad [1.14]$$

Knowing that D_h is equal to 2 h, by defining a Fourier number Fo = at / h^2, we obtain the time t for which both heat fluxes are equal. This is the time t such that:

$$Fo = 0.78\left(\frac{x}{Pe.D_h}\right)^{\frac{2}{3}} \quad [1.15]$$

Let us apply this relationship to the results displayed in Figure 1.9. We remind that the Peclet number is Pe = 1.2. 10^4, D_h = 2h = 6.10^{-3}m, and the sensor F1 is at x = 67 mm from the gate. The diffusivity is a = 2.5.10^{-7} $m^2.s^{-1}$. This gives a time t = 0.27 s. If it is added to the time of passage in front of the sensors, we obtain the end of the shock regime between 0.65 and 0.7 s. It is seen in Figure 1.9 that this time corresponds remarkably well with the beginning of the plateau.

If we perform the same exercise on the SWIM mold of section 1.2.1, we also obtain very interesting results. Figure 1.10 presents the position of the sensors on the wall of the SWIM molding cavity. The closest one is at x = 17 mm to the gate. Figure 1.11 (extracted from [LEB 98]) depicts the heat flux measured during the injection of a polypropylene in the SWIM mold. We note again that the amplitudes of the heat flux close to the gate and the cavity bottom are almost identical. The filling velocity is estimated from the maximum values of the flux to 0.1 $m.s^{-1}$. If we assume an Oswald–de Waelde-type rheological behavior for the PP, the power law index is close to 0.3 (0.308 for the studied PP). The diffusivity is 8.7.10^{-8} $m^2.s^{-1}$. The Peclet number is thus equal to 6,900. We apply the same approach as for the BMC, noting that the expression $\left(\frac{3m+1}{4m}\right)^{\frac{1}{3}}$ now has the value 1.16. A value close to the one obtained for the BMC, which differs only by 5%. This parameter has little importance on the transition between the two regimes. The calculation gives

a time t = 0.454s for equality between the two terms of the heat flux, and therefore the transition between regimes. We see in Figure 1.11 that the filling is finished at this time. We conclude that the whole filling occurs during the heat shock regime.

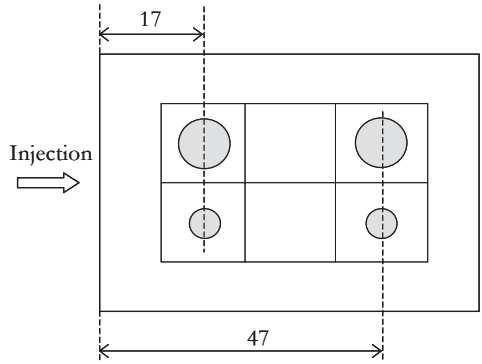

Figure 1.10. *Position of the sensors on the mold SWIM*

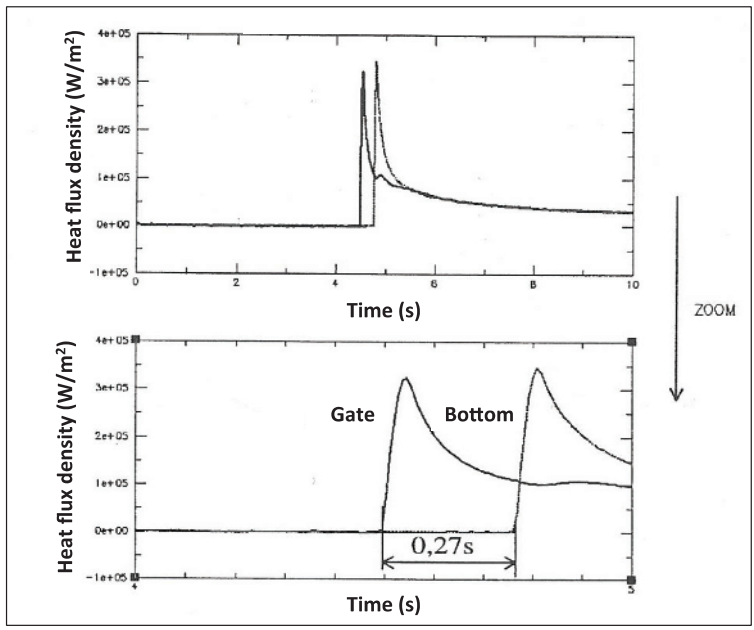

Figure 1.11. *Heat flux density during the passage of the molten PP in front of the sensors*

Finally, considering a domain of variation of the power law index including most of the injected polymers, we are able to propose a criterion determining the transition between the regimes. If a Fourier number Fo, built on the thickness of the piece and estimated at a distance x from the molding cavity gate, satisfies:

$$\mathrm{Fo} < 0.6 \left(\frac{x}{Pe.D_h}\right)^{\frac{2}{3}} \qquad [1.16]$$

Then, it can be considered that the regime of heat shock prevails at this location. This equation takes into account the range of variation of the power law index of the polymer-based pastes.

1.2.2. *Heat transfer during part consolidation*

1.2.2.1. *Consolidation of the thermoplastic parts*

During the consolidation phase, new phenomena must be taken into account. A very strong coupling exists between the heat transfer and the phase change in the case of semi-crystalline. The coupling is initially induced by a strong dependence of thermophysical properties on temperature, pressure and the physical state, i.e. liquid or solid (including the crystalline fraction). These properties are the specific volume, the specific heat and the thermal conductivity. We will discuss this in Chapter 2, but it can be said that these data are accessible with suitable apparatuses. The term of compressibility may be non-negligible, especially when the pressure varies very quickly at the commutation time in injection molding (temperature rise of few degrees). Viscous dissipation is generally negligible because of the low flow velocities in these phases. The source term must be of course taken into account adequately for semi-crystalline polymers. It is related to the kinetics of crystallization and its release participates in the coupling between the phase change and heat transfer. Provided that the homogenization is possible in the composite, the source is weighted by the weight fraction of the matrix. This question of homogenization is not trivial and research works remain to be undertaken to indicate in which circumstances it is possible. The coupling between the heat transfer and crystallization is controlled by the ratio of two characteristic times called thermal Deborah number *De*. This is the ratio between the characteristic time of heat transfer $\tau = e^2/a$, where *e* is a characteristic length of the part and *a* is the thermal diffusivity (typically 1.10^{-7} $m^2.s^{-1}$) and the characteristic time of the transformation t_t at the temperature where it occurs in the core of the part. We can choose the transformation half-time t_c, which is accessible experimentally. Let us take the example of a PP part with a half-thickness equal to 2 mm. Crystallization occurs at 100°C, the crystallization half-time is 1 s, which is small compared to τ = 40 s.

Depending on the value of *De*, one can fall in one of the three situations illustrated in Figure 1.12.

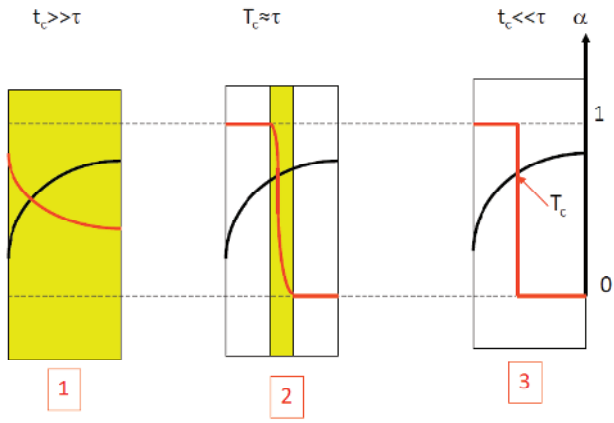

Figure 1.12. *Coupling between the temperature and phase change fields. The temperature field is in black and the transformation field is in red. For a color version of the figure, see www.iste.co.uk/boyard/heat.zip*

Of course, solid and liquid Stefan numbers defined in section 1.2.1.1 play a role in the coupling. If these numbers are large, the heat source is negligible and heat transfers are the same as those in a part made with anamorphous thermoplastic. If Stefan numbers are small, the thermal behavior will depend on the characteristics time ratio. If *De* is very large, the polymer behaves like two phases with a localized (sharp) interface, and the change of state occurs at T_c (case 3, in Figure 1.12). A plateau is observed at T_c on the temperature evolution in the centre of the part. This is almost true for the solidification example given above for a PP, for which De = 40. If $De \approx 1$, there is a quasi-plateau of phase change in the core of the part and the transformation zone has limited thickness compared to the part one (case 2, Figure 1.12). A good approximation of solidification and cooling times is possible with simplified models already mentioned in section 1.2.1.1 (see [SOB 13]). In the case where the phase change time is large compared to the thermal time constant (case 1 in Figure 1.12), *De* is small and the thermal history imposes locally the phase change. Heat transfer and phase change can be uncoupled. We are then in a case similar to the forming of an amorphous polymer, for which the cooling is easy to model, noting that the time evolution of molding cavity surface temperature shown in Figure 1.3 may be represented by a triangle. The average temperature of the

molding cavity surface during the cycle $\overline{T}_s$ can then easily be determined and used in a conventional analytical solution to calculate the cooling time.

Kinetic laws, which provide the relationship between the rate of transformation $d\alpha/dt$ to the temperature and the transformed fraction α (see Chapter 3), are used to make the coupling between the energy conservation equation and the equation which describes the evolution of the transformed fraction. Indeed, the source in the energy equation, related to the phase change, is:

$$Q = \rho\,(P, T, \alpha)\,\Delta H\,\partial\alpha/\partial t \qquad [1.17]$$

In this expression, ρ is the density and ΔH is the phase change enthalpy.

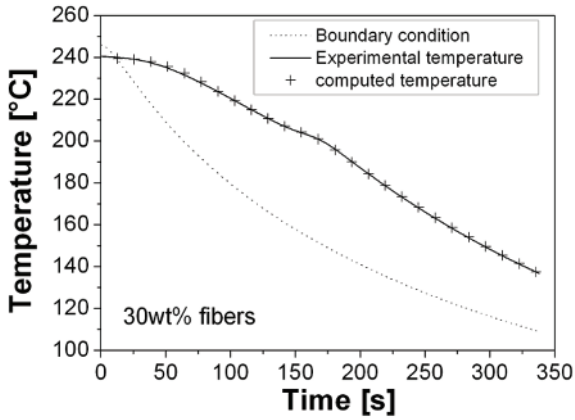

Figure 1.13. *Measured and calculated temperature during the solidification of a reinforced poly-aramide (IXEF 1002)*

The kinetics is piezo-dependent: the increase in pressure moves the crystallization toward higher temperatures. The heat source is thus released at temperatures, which depend on the pressure and this has a strong impact on the temperature fields. Many formulations are available for the source and the readers will find a detailed presentation later in this book (Chapter 3). Nevertheless, it is observed that the temperature difference called supercooling: $\Delta T = T_m^0 - T$ appears in the expression of the crystallization kinetics. The temperature T_m^0 refers to the thermodynamic melting temperature. The effect of pressure on the kinetics is related to the increase in the thermodynamic melting temperature when the pressure P increases, which has to be taken into account in the expression for the kinetics [LEG 10, FUL 01]. Figure 1.13 shows the excellent agreement between simulated

and measured temperatures in the core of the part [LEG 11]. The modeling of heat transfer includes crystallization heat source, including the pressure effect. Similar results are obtained for a composite polyamide/UD glass fiber [FAR 15]. The cooling rate decreases (quasi-plateau) during the crystallization. It should also be noted that this level of accuracy requires a good modeling of the thermal properties, in particular depending on the phase change, which will be discussed in Chapter 2.

1.2.2.2. *Part consolidation with a thermosetting matrix*

The problem is identical to the previous one for the thermosetting matrix composites. It can be estimated that the calculation of the temperature fields coupled to the source of polymerization (cross-linking) is now performed correctly, subject to a number of precautions, especially related to a good estimate of the thermal properties and their changes according to the degree of conversion [DEL 14a, DEL 14b]. An example of the level of accuracy in the prediction of coupled fields is shown in Figure 1.14 [BAI 98].

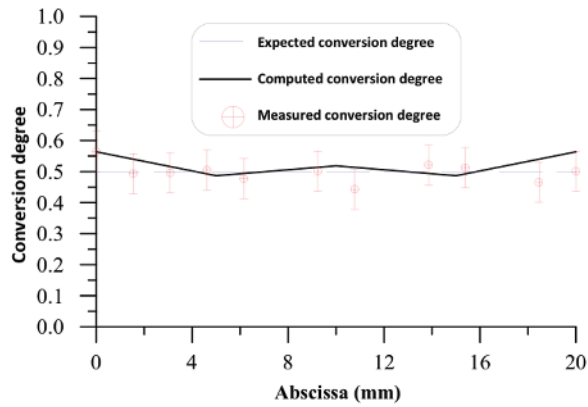

Figure 1.14. *Comparison between the measured and calculated conversion degree in an epoxy/UD glass fiber part in which partial and uniform polymerization was carried out through the thickness [BAI 98]*

Indeed, the solved problem included an inverse method to compute the optimized temperature cycle to impose on the surfaces of a 10 mm thick plate of composite epoxy/glass fiber to obtain a uniform and partial conversion degree in the thickness of the plate. Of course, the accurate knowledge of the cross-linking kinetics is mandatory since it is necessary to avoid uncontrolled heating in the centre of the part, linked to the release of the heat due to the chemical reaction in such an insulating medium. The conversion degree was verified by cutting small strips in the thickness of the plate and then measuring the residual enthalpy by DSC. It is seen

that the control of the transformation with an optimized temperature cycle, which is very difficult to achieve, is efficient and a partial predetermined state of cure can be reached with a good accuracy.

1.3. Injection on continuous fiber reinforcements

This problem is particular. In this section, we are discussing about process of the type liquid composite molding (LCM), for which continuous reinforcement is placed in the mold, which is closed, and then the resin is injected to impregnate the preform. An alternative is to partially close the mold, such as in C-RTM, to impregnate the reinforcement with a transverse flow in the thickness. This is, first of all, multi-scale medium: the microscopic scale is associated with the fibers and meshes (10–100 μm), the mesoscopic scale is related to the ply (millimeter scale) and finally the macroscopic scale is associated with the part (meter is the order of magnitude). Chapter 6 will deal with homogenized transfer equations in such a medium. During the consolidation of parts, problems are identical to those presented in the previous section. A new generation of composite arises now, based on thermoplastics. This is of great interest, because of their ecological potential (recycling, bio-based polymers), the possible reduction of the forming cycle, the lack of post-curing, their potential welding and post-forming and their increased mechanical properties (impact resistance). The high viscosity of thermoplastic polymers raises the difficulty of impregnating continuous reinforcement with a viscous polymer. Two solutions are thus possible to overcome this difficulty, either coupling the RTM process and polymer chemistry by injecting a monomer onto the reinforcement, polymerization (to create macromolecules) and crystallization are then produced in the mold, or injecting low viscosity polymers which then crystallize in the mold. Both ways are developed by polymer suppliers, raising many scientific and technological obstacles. Indeed, the challenges are numerous for parts manufacturers: to achieve as fully as possible the polymerization in the case of reactive injection, to achieve an optimum crystallinity, to obtain a composite with controlled porosity (air/water), to control shrinkage induced by transformations, to get a good surface aspect, to ensure reasonable cycle times depending on the application (including automotive) and finally to develop an “industrial” process. Scientifically, the challenges are no less pithy: the first one is to understand and control the coupling between crystallization and polymerization: from a certain conversion, the polymer will crystallize, hindering the macromolecule growth. There is a competition between both mechanisms that have to be controlled by an accurate temperature control.

Obtaining a composite with controlled porosity supposes an understanding of how the double scale flow evolves, within and between the meshes of a fluid whose chemo-rheological properties vary with the time and the temperature changes due to

heat transfer. The lack of knowledge on mechanisms provokes a bad impregnation and voids caused by air, reaction gas and/or water bubbles entrapment. The situation is generally observed and analyzed in [VIL 15, NOR 12, RUI 12] for example, and is also schematically shown in Figure 1.15.

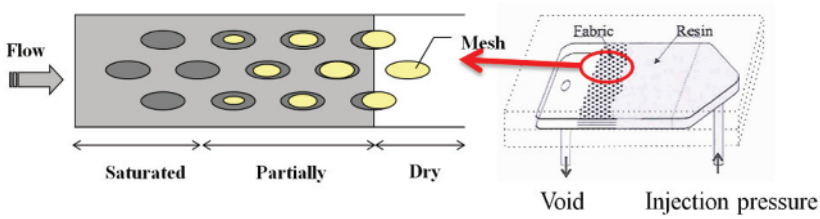

Figure 1.15. *Saturated and unsaturated flows into the fabric of a composite part during the impregnation of a continuous reinforcement (fluid is in yellow). For a color version of the figure, see www.iste.co.uk/boyard/heat.zip*

a)

b)

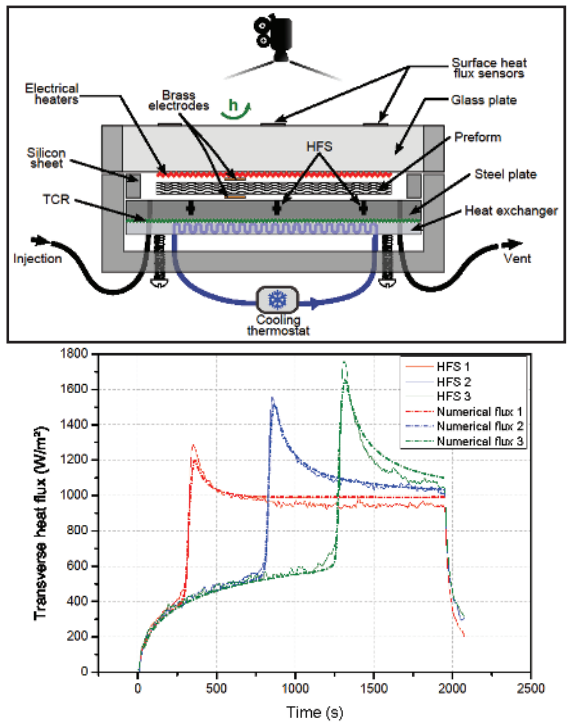

Figure 1.16. *a) Experimental bench and b) recorded and calculated heat flux at the sensor locations [VIL 15] . For a color version of the figure, see www.iste.co.uk/boyard/heat.zip*

According to the respective velocity of impregnation between the meshes and in the meshes, air bubbles can be trapped in the composite, therefore degrading its quality. Modeling heat transfer in and through the structure during the impregnation has been addressed by the heat transfer community and is an important scientific challenge. It should be noted that the thermal conductivity has a high sensitivity to the saturation [VIL 15], but it varies in a differentiated manner depending on the intra-mesh or inter-mesh saturation. Nevertheless, it has been shown that the heat transfer modeling can be performed with a good accuracy. This is illustrated in Figure 1.16(b) that shows the comparison between the simulated and measured heat flux when a known heat flux is dissipated by a thin heater on the wall of a mold, in which of a fluid impregnates the reinforcement, as shown schematically in Figure 1.16(a).

When the flow front reaches the sensor position, the heat flux sharply increases and then decreases until it reaches a value corresponding to the established convective regime. We can see in this figure the very good agreement between the measured and calculated heat flux, the latter taking into account both the heat transported by the flow and that passing through the composite thickness during the saturation. Another phenomenon must be taken into account and is known as thermal dispersion. It appears when the temperature and flow rates at the microscopic scale are different from their mean values. Physically speaking, local convection phenomenon between meshes increases the effective thermal conductivity. It is then necessary to include the effect of tortuosity. During the tortuous flow between the meshes, in the presence of a transverse temperature gradient in particular, heat is transported in a complex way, resulting in an increased apparent thermal conductivity. Lecointe [LEC 99] shows that we must introduce a dispersive thermal conductivity λ_d, which depends on the Peclet number built on the hydraulic diameter of the inter-meshes channels. However, some problems remain open today in this field: the thermal homogenized conditions of entry and the modeling of a coupled heat transfer-unsaturated multi-scale flow. On the contrary, the consolidation phase is solved, it is identical to the case described in the previous section, provided that a correct coupling between the polymerization reactions (identical to the case of thermosets) and the crystallization exists, which can be influenced by the shear in the meshes and the confinement between the fibers (transcrytallinity).

1.4. Conclusion: toward a controlled processing

As can be seen in this chapter, many problems related to heat transfer during composite processing were solved during numerous studies dedicated to this topic. Heat transfers during the filling of short fiber composites are well described by the

models, provided that the orientation tensor is, of course, correctly estimated. The consolidation is also described satisfactorily, the coupling with the transformation kinetics (polymerization or crystallization) allowing us to accurately estimate the overheating due to the source release during the transformations. Many challenges are still to be met. Without being exhaustive, these challenges include the problem of modeling the non-isothermal saturation of the reinforcing fabrics, taking into account the influence of shear on the crystallization at the various scales of these reinforcements, the influence of shear on the thermal conductivity (effects of anisotropy by the orientation of the macromolecules or the crystalline structures), the contact resistance between a part and a tool, or between plies, the adequate consideration of radioactive effects in semi-transparent medium (for example, composite PA/glass fibers). Finally, advances in thermal metrology in the composite processing to validate the models, especially to measure composite surface temperatures, temperatures inside the composite without intrusivity or also 2D heat flux fields. Once these many challenges are confronted, we can extend the works to thermomechanical coupling to optimize the processing parameters to meet criteria on the residual stresses and war pages.

1.5. Bibliography

[BAI 98] BAILLEUL J.L., DELAUNAY D., JARNY Y., "Optimal thermal processing of composite materials, an inverse algorithm and its experimental validation", *11th International Heat Transfer Conference*, pp. 87–92, 1998.

[CAR 59] CARSLAW H.S., JEAGER J.C., *Conduction of Heat in Solids*, 2nd ed., Oxford University Press, London, 1959.

[DEL 11] DELAUNAY D., "Thermal conductivity of an injected polymer and short glass fibers composite part: measurement and model", *Keynote in 27th world Congress of the polymer Processing Society*, Marrakech, pp. KN–15–517, 2011.

[DEL 14a] DELAUNAY D., SOBOTKA V., THOMAS S. *et al*., "Thermal properties", in THOMAS C., SINTUREL, THOMAS R. (eds), *Micro and Nanostructured Epoxy/Rubber Blends*, Wiley-VCH, 2014.

[DEL 14b] DELAUNAY D., BOYARD N., "Pressure-volume-temperature (PVT) analysis", in THOMAS S., SINTUREL C., THOMAS R. (eds), *Micro and Nanostructured Epoxy/Rubber Blend*, Wiley-VCH, 2014.

[FAR 15] FARAJ J., PIGNON B., BAILLEUL J.L. *et al*., "Heat transfer and crystallization modeling during compression molding of thermoplastic composite parts", *Key Engineering Materials*, vols. 651–653, pp. 1507–1512, 2015.

[FUL 01] FULCHIRON R., KOSCHER E., POUTOT G. *et al*., "Analysis of the pressure effect on the crystallization kinetics : dilatometric measurements and thermal gradient modelling", *Journal of Macromolecular Science: Physics*, vol. B40, pp. 297–394, 2001.

[LE 07] LE T.H., ORGEAS L., FAVIER D. *et al*., Rhéologie des BMC lors de leur injection, Compte-rendu du 18ème Congrès de Mécanique, 2007.

[LEB 98] LE BOT P., Comportement thermique des semi-cristallins injectés. Application à la prédiction des retraits, PhD Thesis, University of Nantes, 1998.

[LEC 99] LECOINTE D., Caractérisation et simulation des processus de transferts lors d'injection de résine pour le procédé RTM, PhD Thesis, University of Nantes, 1999.

[LEG 06] LE GOFF R., Etude et modélisation des transferts thermiques lors de la solidification de pièces injectées en polymère semi-cristallin chargé de fibres, PhD Thesis, University of Nantes, 2006.

[LEG 10] LE GOFF R., BOYARD N., SOBOTKA V. *et al*., "A heat transfer analysis of injection molding of fiber-reinforced poly (M-xylylene Adipamide)", *International Journal of Material Forming*, vol. 3, no. 1, pp. 805–808, 2010.

[LEG 11] LE GOFF R., BOYARD N., SOBOTKA V. *et al*., "Inverse estimation of the crystallization kinetic function of semi-crystalline polymers and short fiber reinforced composites in moderate cooling conditions", *Polymer Testing*, vol. 30, pp. 678–687, 2011.

[LOU 97] LOULOU T., DELAUNAY D., "The interface temperature of two suddenly contacting bodies, one of them undergoing phase change", *International Journal of Heat and Mass Transfer*, vol. 40, no. 7, pp. 1713–1716, 1997.

[PIN 09] PINHO F.T., COELHO P.M., *Non-Newtonian Heat transfer in Rheology*, Encyclopedia of Life Support Systems, Eolss Publishers, Oxford, UK, 2009.

[MIL 01] MILLISCHER A., DELAUNAY D., "Experimental and numerical analysis of heat transfer in bulk molding compound injection process", *Journal of Reinforced Plastics and Composites*, vol. 20, no. 6, pp. 495–512, 2001.

[NOR 12] NORDLUND M., MICHAUD V., "Dynamic saturation curve measurement for resin flow in glass fibre reinforcement", *Composites Part A*, vol. 43, no. 3, pp. 333–343, 2012.

[QUI 98] QUILLIET S., Transferts thermiques à l'interface polymère métal dans le procédé d'injection des thermoplastiques, PhD Thesis, University of Nantes, 1998.

[RUI 12] RUIZ E., LEBEL F., TROCHU F., "Experimental study of capillary flows, voids formation and void migration in LCM manufacturing", *11th Flow Processes in Composite Materials*, pp 136–143, 2012.

[SOB 13] SOBOTKA V., AGAZZI A., BOYARD N. *et al*., "Parametric model for the analytical determination of the solidification and cooling times of semi-crystalline polymers", *Applied Thermal Engineering*, vol. 50, pp. 416–421, 2013.

[SOM 12] SOMÉ S.C., GAUDEFROY V., DELAUNAY D., "Estimation of bonding quality between bitumen and aggregate under asphalt mixture manufacturing condition by thermal contact resistance measurement", *International Journal of Heat and Mass Transfer*, vol. 55, pp. 6854–6863, 2012.

[VIL 15] VILLIERE M., GUEROULT S., SOBOTKA V. *et al*., "Dynamic saturation curve measurement in liquid composite molding by heat transfer analysis", *Composites Part A*, vol. 69, pp. 255–265, 2015.